Biochimica et Biophysica Acta 1827 (2013) 793–805

Contents lists available at SciVerse ScienceDirect

Biochimica et Biophysica Acta

journal homepage: www.elsevier.com/locate/bbabio

Deletion of β-strands 9 and 10 converts VDAC1 voltage-dependence in an asymmetrical process

Simona Reina [a,b], Andrea Magrì [a,b], Marco Lolicato [c], Francesca Guarino [a,b], Agata Impellizzeri [a,b], Elke Maier [d], Roland Benz [d,e], Matteo Ceccarelli [f], Vito De Pinto [a,b], Angela Messina [a,b,*]

[a] Department of Biological, Geological and Environmental Sciences, Section of Molecular Biology, University of Catania, Italy
[b] National Institute for Biomembranes and Biosystems, Section of Catania, viale A. Doria 6, 95125 Catania, Italy
[c] Department of Biology, University of Milano, 20133 Milano, Italy
[d] Rudolf-Virchow-Center, DFG-Research Center for Experimental Biomedicine, University of Würzburg, D-97078 Würzburg, Germany
[e] School of Engineering and Science, Jacobs University Bremen, Campusring 1, 28759 Bremen, Germany
[f] Department of Physics and IOM-CNR, University of Cagliari, 09042 Monserrato, Italy

ARTICLE INFO

Article history:
Received 9 November 2012
Received in revised form 6 March 2013
Accepted 18 March 2013
Available online 28 March 2013

Keywords:
Mutant protein
Voltage dependent anion channel
Voltage gating process
Molecular dynamics simulation

ABSTRACT

Voltage-dependent anion selective channel isoform1 maintains the permeability of the outer mitochondrial membrane. Its voltage-gating properties are relevant in bioenergetic metabolism and apoptosis. The N-terminal domain is suspected to be involved in voltage-gating, due to its peculiar localization. However this issue is still controversial. In this work we exchanged or deleted the β-strands that take contact with the N-terminal domain. The exchange of the whole hVDAC1 β-barrel with the homologous hVDAC3 β-barrel produces a chimeric protein that, in reconstituted systems, loses completely voltage-dependence. hVDAC3 β-barrel has most residues in common with hVDAC1, including V143 and L150 considered anchor points for the N-terminus. hVDAC1 mutants completely lacking either the β-strand 9 or both β-strands 9 and 10 were expressed, refolded and reconstituted in artificial bilayers. The mutants formed smaller pores. Molecular dynamics simulations of the mutant structure supported its ability to form smaller pores. The mutant lacking both β-strands 9 and 10 showed a new voltage-dependence feature resulting in a fully asymmetric behavior. These data indicate that a network of β-strands in the pore-walls, and not single residues, are required for voltage-gating in addition to the N-terminus.

1. Introduction

The voltage-dependent anion channel (VDAC) is the most abundant integral membrane protein of the mitochondrial outer membrane and forms hydrophilic pore structures [1–3]. It is considered a key regulator of metabolite flow as the preferred exchange route of adenosine nucleotides from and to the mitochondrion [4]. VDAC is also co-responsible in various cell processes including apoptosis [5–8] and calcium homeostasis [9,10] and it has been recently indicated as a target for anti-cancer therapies [11–14]. Its responsibility in apoptosis is well recognized, even though there is a debate about the mechanism of action [15]. Deficiency of VDAC has been associated with a lethal encephalomyopathy [16]. Any eukaryotic genome contains a little collection of VDAC genes that, despite a high level of conservation and an evident common evolutionary origin [17,18], shows a composite set of slightly different functional features. In vertebrates three functional genes encode different VDAC isoforms (named VDAC1, 2 and 3) [19]. Functional experiments demonstrated that recombinant VDAC1 and VDAC2 are able to form pores in lipid bilayers, different from VDAC3 that shows a reduced pore-forming ability [20,21].

The most important regulatory feature of VDAC is voltage-dependence. Voltage-dependence has been discovered in vitro, in reconstitution experiments in artificial bilayer: VDAC channel exists in a high conductive state when the applied voltage is close to 0 mV. Upon higher voltages (>20 mV) VDAC switches to lower conductance states [22]. These states are associated with changes in the structural organization [22–24] and hitherto in the permeability features of the pore: since ion and metabolite permeation is affected by the voltage-dependence, open and closed states of the VDAC pore have been consequently defined [25]. The closed state is still permeable to small ions but not to larger molecules like ATP and ADP [4]. A structural detail of this relevant feature is still missing nowadays, despite that structural models of human [26,27] and

* Corresponding author at: Department of Biological, Geological and Environmental Sciences, Section of Molecular Biology, University of Catania, Italy. Tel.: +39 095 7384231; fax: +39 095 7384243.
E-mail address: mess@unict.it (A. Messina).

0005-2728/$ – see front matter © 2013 Elsevier B.V. All rights reserved.
http://dx.doi.org/10.1016/j.bbabio.2013.03.007

mouse VDAC1 [28] have been reported. In these structures VDACs are formed by an almost completely antiparallel β-barrel containing 19 amphipathic β-strands joined to an N-terminal sequence of variable lengths, mainly formed by amphipathic α-helix segments [26–28]. These 3D structures agree on the location of the N-terminal inside the pore, even with some differences. Another report questioned this structure and proposed a different 3D arrangement of the protein on the basis of electrophysiological experiments [29]. It has to be clarified which one of the two models corresponds to the cellular structure or whether they can both exist as different states of the pore [29,30].

These structural–functional debates prompted several studies. In particular a general interest is focused on the very peculiar location of the N-terminal domain that suggests a putative gating function. In a very first work on the synthetic peptide of N-terminal hVDAC1 sequence [31] it was showed that the organized secondary structure of the N-terminal is only possible when it is constrained by charges and/or a hydrophobic environment. A recent solid-state NMR analysis [32] of hVDAC1 sustained that the N-terminus adopts a well-defined α-helical conformation remarkably similar to the mVDAC1 crystal. The contacts of this helix with the wall-pore β-strands are considered important to maintain the stability of the pore structure [32]. In contrast, another work reported that the strands opposed to the α-helix (β2, β5, β18 and β19) are less dynamic than others (β8 and β15) [33] and that the overall channel structure is stabilized by the interactions between the walls and the apposed α-helix. The role of other residues, like a network of Lysines, in close proximity to the Thr6 residue, has recently been highlighted. Stabilizing contacts between the α-helix and the β-strands have been also attributed to hydrophobic interactions among the residues L10, V143 and V150 [32,33]. The identification and the possibility to interfere with the interactions between N-terminal and the pore walls are considered a crucial feature to understand how voltage-gating works [32–34].

In this work we studied the influence of the contacts between the N-terminal sequence and β-strands facing it. This influence was monitored by looking for difference in voltage-dependence and ion selectivity features of the protein. For this purpose we did not restrict our work to site-directed mutagenesis of single residues but instead we changed large sections of the inner wall of the pore. In a former mutant we changed the whole β-barrel in front of the hVDAC1 N-terminal α-helix substituting the hVDAC1 barrel with the homologous but not identical hVDAC3 barrel. In other mutants we deleted in hVDAC1 the whole β-strand 9 or the hairpin of β-strands 9 and 10, thus removing the strands responsible of these contacts. Mutants were expressed, purified and reconstituted in artificial planar bilayers. Strikingly the deletion of these strands is responsible of an asymmetrical change in the voltage-dependence of the pore.

2. Materials and methods

2.1. Yeast strains, growth conditions and hVDAC expression

Wild type *Saccharomyces cerevisiae* strain BY4742 [MAT a, his3Δ1, leu2Δ0, lys2Δ0, ura3Δ0] and isogenic porin-depleted mutant Δpor1 [MATa, his3Δ1, leu2Δ0, lys2Δ0, ura3Δ0, por1::kanMX4] were obtained from EUROSCARF (Frankfurt, Germany). Rich media for yeast growth contained 1% yeast extract, 2% peptone and 2% glucose. Synthetic media (containing the appropriate nutritional supplements for auxotrophs) were as described [35,36].

2.2. hVDAC expression and purification from yeast

N1-VDAC3 (chimeric hVDAC3 containing the N-terminus of hVDAC1), hVDAC1 and hVDAC3 were cloned in the *yeast—Escherichia coli* shuttle vector pYX212 (Novagen) and expressed in Δpor1 cells as previously reported [21].

Isolation of mitochondria was performed as described by Gregg et al. [37]. Briefly, cells (1 l culture) were harvested by centrifugation (5 min, 3000 ×*g*) and washed twice with water. The cell pellet was resuspended in DTT buffer (100 mM Tris/H_2SO_4 pH 9.4, 10 mM DTT) and the cell suspension was rotated for 20 min at 30 °C. After centrifugation (5 min, 3000 ×*g*) the pelleted cells were resuspended in Zymoliase buffer (20 mM potassium phosphate pH 7.4, 1.2 M sorbitol, zymoliase 100 T) and rotated for 30 min at 30 °C. Spheroplasts were centrifuged (8 min, 2200 ×*g*) and resuspended in homogenization buffer (10 mM TrisHCl pH 7.4, 0.6 M sorbitol, 1 mM EDTA, 0.2% BSA). The suspension was disrupted with a pestle and the obtained supernatant containing mitochondrial fraction was centrifuged (12,000 ×*g*, 15 min). Mutant and native hVDACs were released from the mitochondrial fraction by LDAO-extraction as described in [38], and were subsequently purified by HTP/celite 2:1. Protein concentration was determined using Bradford method.

2.3. Construction of mutants hVDAC1Δβ9 and hVDAC1Δβ9-β10

Mutagenesis was performed onto the hVDAC1 coding sequence cloned in pYX212. *E. coli* strain XL10Gold was utilized in gene construction. Removal of β9 and β10 from human VDAC1 sequence was achieved by PCR-based gene deletion strategy as described in [39,40]. Two primers flanking the codons for amino acids 136 and 147 were used to delete β9: forward 5′-GACATTGCTGGGGGCTGGCTGGCCGGCTAC-3′ and reverse 5′-GGCCAGCCAGCCCCCAGCAATGTCGAAATC-3′. Two primers flanking the codons for amino acids 136 and 160 were used to delete both β9 and β10: forward 5′-GACATTGCTGGGAAATCCCGAGTGACCCAG-3′ and reverse 5′-CACTCGGGATTTCCCAGCAATGTCGAAATC-3′. PCR fragments were cut with the restriction enzymes *NdeI* and *XhoI* and cloned, together with hVDAC1 wild type, into the pET21a vector (Novagen). The sequences of the mutant proteins were confirmed by DNA sequencing.

2.4. Heterologous hVDAC expression and purification

Recombinant His-tagged proteins were expressed in *E. coli* BL21 (DE3). Bacteria were grown at 37 °C to an A_{600} of 0.6 and protein expression was induced with isopropyl β-D-1-thiogalactopyranoside for 3 h at 37 °C. Following centrifugation, pellet was resuspended in buffer B (8 M Urea, phosphate buffer, pH 8.0) and overnight shaken at 4 °C. After pelleting cell debris by centrifugation, the clear lysate was purified by chromatography using nickel-nitrilotriacetic acid resin (Ni-NTA, Qiagen). The purified proteins were eluted with buffer B (pH 3.5).

2.5. VDAC refolding

To obtain hVDAC proteins with full biological activity, on-column refolding affinity chromatography was used [41]. One milliliter of Talon resin (Clontech) pre-equilibrated with buffer B (0.1 M NaH_2PO_4, 0.01 M TrisHCl, 8 M urea pH 8.0) was loaded with 2 ml denatured protein supernatant (containing ~3 mg purified hVDAC) previously led to pH 8. The column was washed once with buffer B mixed with buffer C (25 mM NaPi pH 7.0, 100 mM NaCl, 2% LDAO, [3]) plus 10 mM imidazole (B:C 1:3) and two times with buffer B mixed with buffer C^1 (25 mM NaPi pH 7.0, 100 mM NaCl, 1% LDAO) plus 10 mM imidazole (B:C^1 1:7 and 1:15 respectively). An additional wash was performed with 20 volumes of buffer C^2 (25 mM NaPi pH 7.0, 100 mM NaCl, 0.1% LDAO) plus 10 mM imidazole. The His-tagged proteins were eluted with 5 bed volumes of buffer C^2 plus 200 mM imidazole. All the procedures were performed under gravity at 4 °C. To remove imidazole that could create problems in lipid bilayer experiments, the samples were dialyzed against a 100× buffer without imidazole

overnight at 4 °C. Thermo Scientific Slide-A-Lyzer Dialysis Cassettes (3.5 K MWCO) were used to avoid any sample loss. The protein purity was verified by 12% SDS-PAGE. The purified proteins were diluted 1:10 in 1% Genapol X-80 (Fluka, Buchs, Switzerland) to prevent aggregation and immediately used for reconstitution experiments.

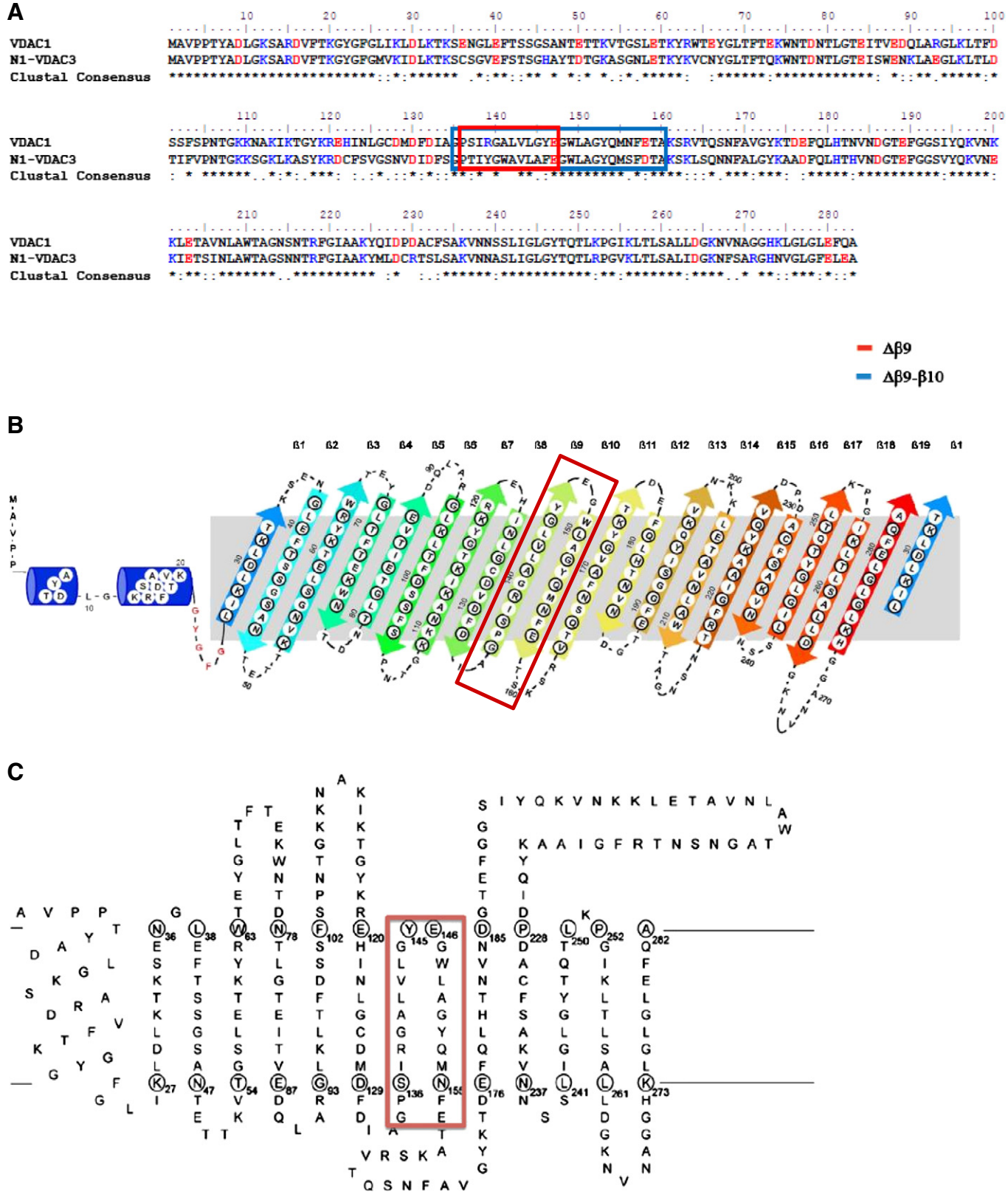

Fig. 1. Features of the mutants used in this work. (A) Alignment of N1-VDAC3 with hVDAC1. Colored boxes indicate the sequences deleted in our experiments. (B) Structure of VDAC according to the crystallographic structure of mVDAC1 [28]. β-strands 9–10 are highlighted by a box. (C) Structure of VDAC according to the model for NcVDAC [29]. β-strands 7–8 (corresponding to β9–β10 in 1B) are highlighted by a box.

2.6. Lipid bilayer experiments

The methods used for black lipid bilayer experiments have been described previously [42]. The experiments were performed at 25 °C. The membranes were formed from a 1% (w/v) solution of diphytanoyl phosphatidylcholine (DiphPC) (Avanti Polar Lipids, Alabaster, Alabama, USA) in n-decane. Bilayer formation was indicated when the membrane turned optically black to reflected light. Mutant and native hVDACs were added from the protein stock solution of 1 mg/ml after the membrane had turned black. The single channel conductance of the pores was measured after application of a fixed membrane potential with a pair of Ag/AgCl electrodes with salt bridges inserted into the aqueous solutions on both sides of the membrane. The stepwise increase in membrane conductance and the voltage-dependency were determined as described [43].

2.7. Modeling of VDAC1Δβ9–β10 mutant

We used all-atom molecular dynamics simulations to build the model of VDAC1 mutant with both β-strands 9 and 10 deleted. We employed the program NAMD-2.8 with the amber 99SB-ildn force field for the protein and the TIP3P model for water [44] and the general amber force field for POPC [45]. We started from the mouse VDAC1 model, for which a high resolution crystal structure is available (PDB ID: 3EMN, 2.3 Å). We eliminated the two β-strands 9 and 10 (from residues 137 to 160) and using Modeller [46] we obtained the starting coordinates. We minimized the structure in the gas phase to allow the closure of the gap between Pro 136 and Lys 161 for 1000 steps, 1 fs timestep and cutoff at 10 Å. At this stage the CO–NH distances between the two strands are in the order of 14 Å.

We imposed such restraints between residues 142–130, 144–128, 146–126, 148–124, and 150–122 with a force constant equal to 10 kcal/(mol* Å^2) and we performed MD simulations in the gas phase at 10 K letting all atoms free to move. Every 10 ps we decreased the restraint distance equilibrium of 1 Å. After a few steps we were obliged to eliminate part of the loop (from 161 to 164) connecting strands 8 and 11 because it was placed in the middle of the two strands. We continued the MD simulations with restraints arriving at a distance of 2 Å, exactly as hydrogen bonds between the two β-strands. Then we used Modeller to add the residues 161–164, previously cut, and we performed other 50 ps MD simulations at 50 K. We removed the restraints and we verified that the β-barrel structure of strands 8 and 11 was kept.

To have a model more closely related to the real system and then more predictive, we embedded the protein in a POPC phospholipid bilayer and we solvated with water, obtaining a system of approximately 51,000 atoms. We performed state-of-the-art MD simulations in the NPT ensemble with periodic boundary conditions and long range electrostatic interactions evaluated with the PME algorithm employing the program ACEMD [47]. We slowly increased the temperature up to 300 K relaxing, at the same time, the box for 10 ns, and arriving, at the end, to an average box dimension of 77.81 × 77.81 × 82.95 Å. We then performed 200 ns in the NVT ensemble and this long trajectory was used for structural analysis saving a structure every 50 ps, or 4000 structures. The same simulation protocol was used to prepare VDAC1 (PDB ID: 3EMN) employed as reference system.

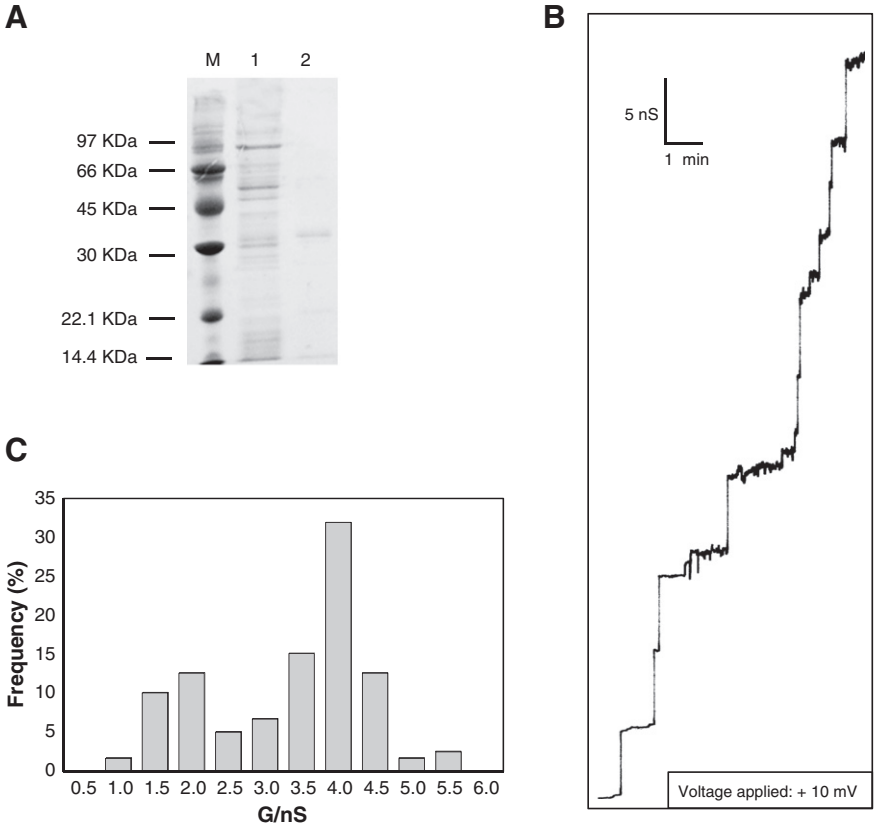

Fig. 2. Electrophysiological characterization of chimeric N1-VDAC3 purified from *S. cerevisiae* mitochondria. A. Electrophoretic analysis of purified hVDAC1 in 12% SDS-PAGE. M: Mr Markers; 2: yeast mitochondrial extract; 3: purified hVDAC1. B. Single channel recording of a DiphPC/n-decane membrane after the addition of hVDAC1 purified from mitochondria of *S. cerevisiae*. The aqueous phase contained 1 M KCl and 25 ng/ml protein. The applied membrane potential was 10 mV; $T = 25$ °C. C. Histogram of the conductance steps measured after reconstitution of hVDAC1 into black lipid bilayer membranes. Conditions as in B. The most frequent single channel conductance was 4 nS for 211 channels. D. Electrophoretic analysis of purified N1-VDAC3 in 12% SDS-PAGE. M: Mr Markers; 2: yeast mitochondrial extract; 3: purified N1-VDAC3. E. Single channel recording of a DiphPC/n-decane membrane after the addition of N1-VDAC3 purified from mitochondria of *S. cerevisiae*. Conditions as in B. F. Histogram of the conductance steps measured after reconstitution of N1-VDAC3 into black lipid bilayer membranes. Conditions as in B. The most frequent single channel conductance was 4 nS for 85 channels.

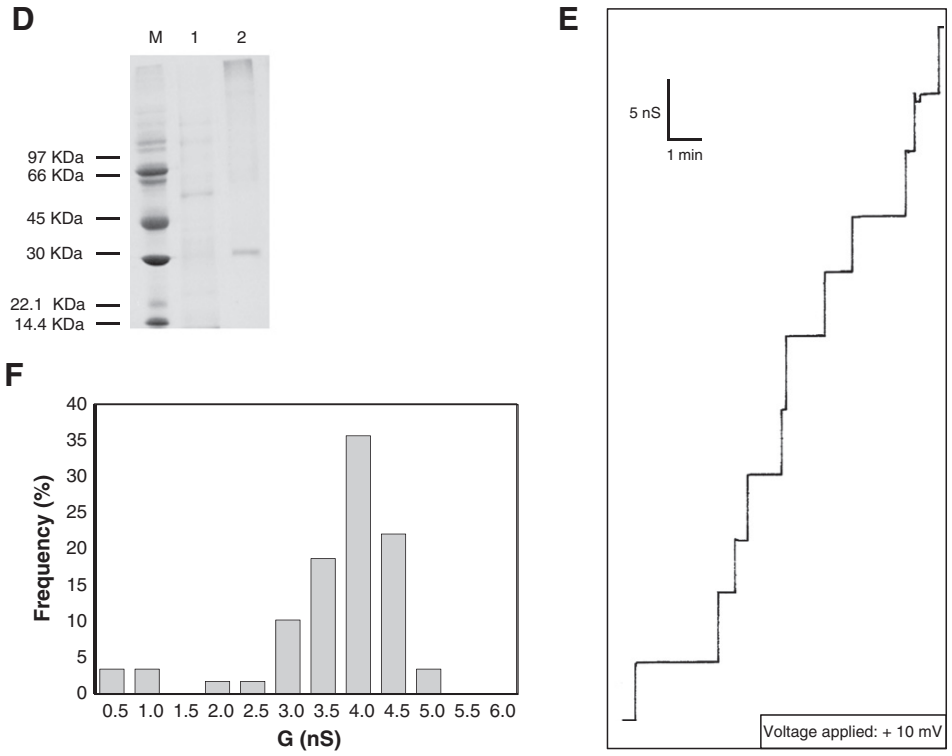

Fig. 2 (*continued*).

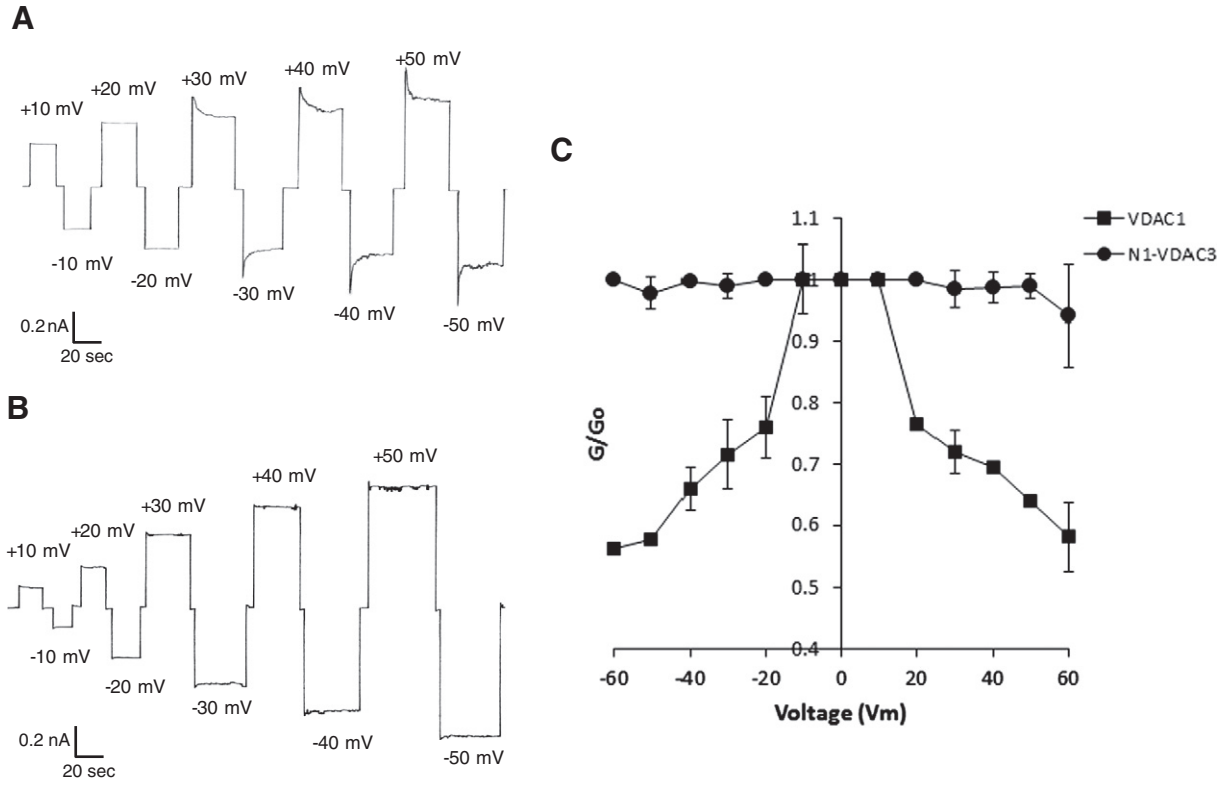

Fig. 3. Voltage-dependence analysis of hVDAC1 and N1-VDAC3. A. hVDAC1 was added to the cis side of a DiphPC/n-decane membrane and the incorporation of several channels with a transmembrane potential of 10 mV was followed until the current remained stable. Next, raising positive and negative voltages were applied to the membrane, and the current was measured as a function of time. The aqueous phase contained 1 M KCl, T = 25 °C. B. Voltage-dependence of N1-VDAC3. Experimental procedure and conditions as in A. C. Analysis of hVDAC1 and N1-VDAC3 voltage-dependence. Ratio of the conductance *G* at a given membrane potential (*V*m) divided by the conductance *G*o at 10 mV was plotted as a function of the membrane potential *V*m. The curves show that hVDAC1 is voltage-dependent (full squares) while the chimera N1-VDAC3 is not. The data shown are the average of three independent experiments.

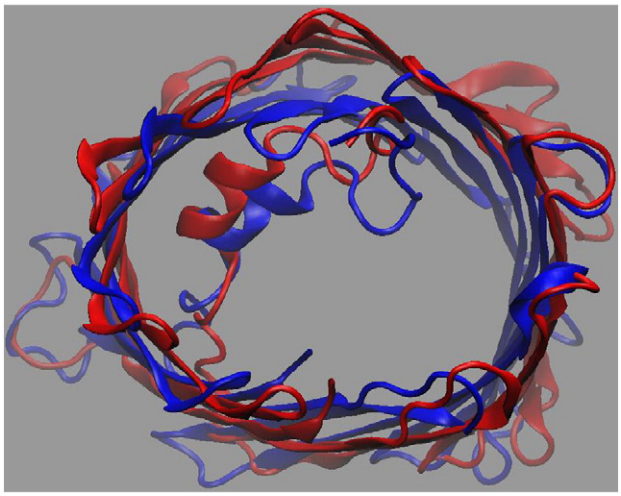

Fig. 4. Top view of the two secondary structures referring to the snapshots extracted after 200 ns simulations and superimposed. In blue the mutant VDAC1Δβ9–β10 and in red the wild type VDAC1 (PDB ID: 3EMN). For clarity, both the bilayer and the water are not shown.

To evaluate the effective size of the pore available for the passage of molecules, we used our own program [48] to calculate all along the axe Z the cross-sectional solvent-accessible surface area (SASA). A 3-dimensional grid of space 0.5 Å, centered on the pore was built. We used a spherical probe of 1.4 Å (modeling a water molecule) rolling on the grid points and the SASA was calculated as the area available to the whole probe. The protein was modeled with van der Waals radii.

3. Results

3.1. The electrophysiological properties of chimeric N1-VDAC3 purified from S. cerevisiae mitochondria

To assess the influence of the β-barrel in its relationship with the N-terminal α-helix we used three constructs. The N1-VDAC3 chimera was produced by insertion of the inactive isoform hVDAC3 β-barrel in place of the hVDAC1 homologous structure [20]. This chimera has been characterized upon yeast cell transformation [21] showing that the simple swapping of the N-terminus is sufficient to re-activate isoform hVDAC3 [21]. Nevertheless its electrophysiological characterization was not accomplished in [21]. Fig. 1A shows the alignment of hVDAC1 with N1-VDAC3. hVDAC1 and hVDAC3 sequences are very similar; in particular, differences in charged residues are very slight: hVDAC1 has 29 acidic residues while both hVDAC3 and N1-VDAC3 have 25 and they both have 35 positive amino acids.

The chimera was purified from mitochondria obtained from the transformed yeast, as in [21]. The expression of the human construct was verified by rt-PCR (not shown). The protocol produced a chimeric protein refolded in a eukaryotic environment.

Table 1
Fitting parameters of the SASA probability distribution function in Fig. 5 for the wild type and mutated VDAC1, as extracted from the 200 ns molecular dynamics trajectory.

Fitting parameters	PDB ID: 3EMN	VDAC1Δβ9–β10
Gaussian height	a0 = 0.0220577	a0 = 0.0248542
Gaussian center	a1 = 191.808	a1 = 69.7379
Gaussian width	a2 = 18.2811	a2 = 16.1835
Chi-square	7.26922e−05	9.34648e−05
Correlation coefficient	0.990637	0.990371
Theil U coefficient	0.095591	0.102173

See Materials and methods section for a discussion of the data.

3.1.1. Single channel analysis

Chimeric N1-VDAC3, and hVDAC1 and hVDAC3 as control, were purified from yeast mitochondria, added to planar phospholipid membranes and studied by electrophysiological methods. hVDAC1 and N1-VDAC3 easily formed channels in a phospholipid membrane. The conductance steps were quite uniform in size and the most frequent single channel conductance event was 4 nS for both N1-VDAC3 and hVDAC1 (Fig. 2). In contrast to hVDAC1 and N1-VDAC3, human VDAC3 formed rarely pores and only very few channels were inserted (data not shown).

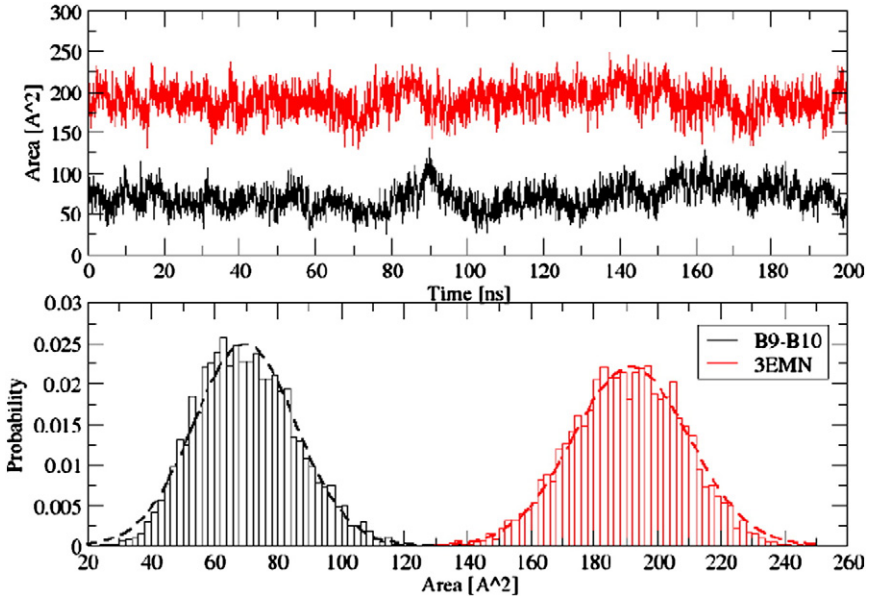

Fig. 5. Minimum value of the SASA for both wt and mutant VDAC1Δβ9–β10 reported as function of time (top) and as normalized probability distribution function (bottom). The SASA (solvent-accessible surface area) has been evaluated using a spherical probe of 1.4 Å radius rolling on a grid of 0.5 Å space and considering the space available to the whole probe.

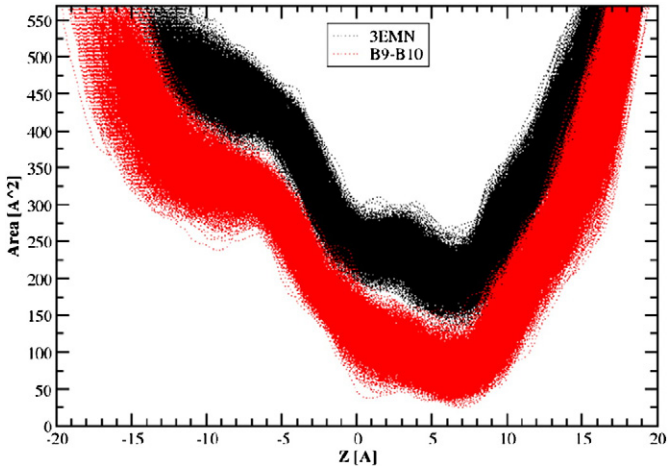

Fig. 6. Accumulated SASA profile as a function of Z in the range [−20:+20] Å.

3.1.2. Voltage-dependence

The voltage-dependence of hVDAC proteins purified from yeast mitochondria was also analyzed. The gating process of hVDAC1 channels and of N1-VDAC3 in response to symmetrical voltage steps of linearly increasing amplitude is reported in Fig. 3. The wild type protein showed the normal voltage-dependent gating activity with the usual symmetrical response to voltage of opposite signs. Channel closure is evident at both positive and negative potentials $> \pm 30$ mV. On the contrary N1-VDAC3 did not show the typical VDAC voltage-dependency. Three independent experiments showed that until ± 90 mV the chimeric protein stays in an open state. Only higher voltages of opposite sign closed the channels (data not shown). Fig. 3C shows the plot of the relative conductance G/G_0 as a function of the applied voltage. The comparison clearly demonstrates the profound differences between the two proteins in terms of gating.

3.2. The chimeric hVDAC1Δβ9 and hVDAC1Δβ9–β10

Deletion of β-strands 9 and 10 was designed on the basis of the crystallographic structure reported in [26–28] (Fig. 1B). These sequences were defined trans-membrane β-strands (numbered 7 and 8 in Fig. 1C) also in the model by Colombini et al. [23,29].

VDAC segments were deleted also in previous works [8,49–52]. Since the sequences deleted in this work are large, and it is possible that such modifications can perturbate the structure, we performed molecular dynamics experiments to probe the stability of the pore.

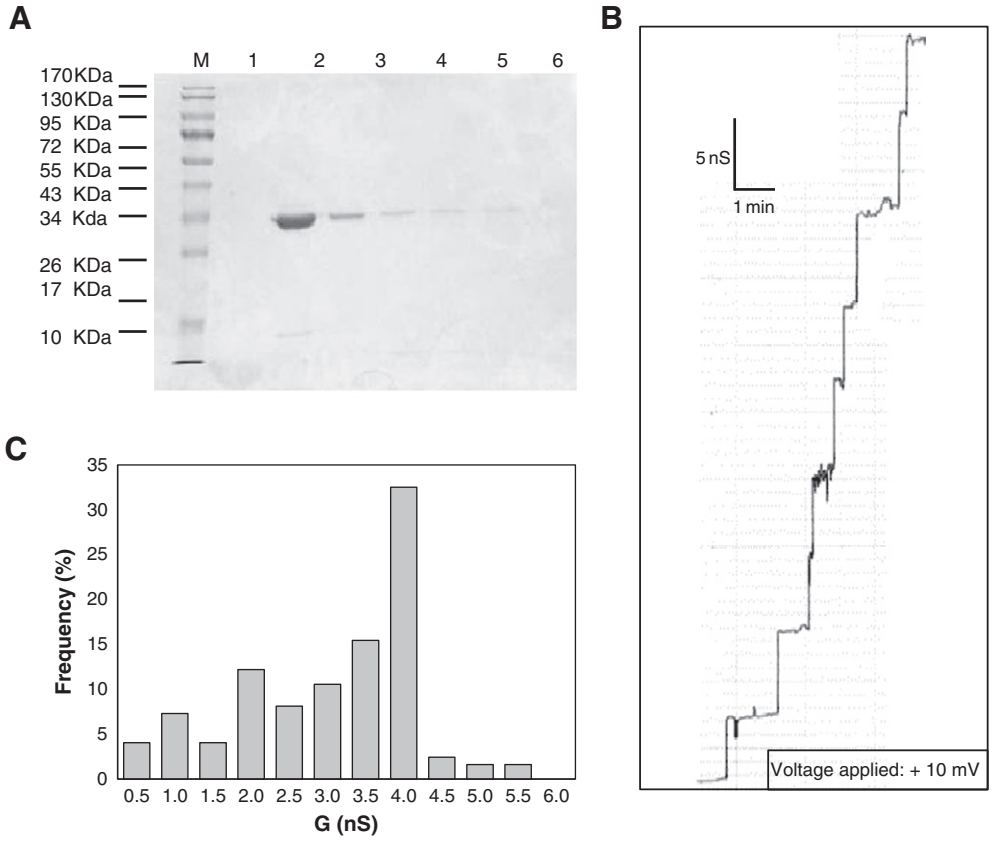

Fig. 7. Electrophysiological characterization of mutants hVDAC1Δβ9 and hVDAC1Δβ9–β10 purified from *E. coli*. A. 12% SDS-PAGE of his-tagged hVDAC1 expressed in *E. coli* and refolded by a Talon column. M: Mr Markers; 1–6: fractions collected from a Talon column showing the purity of hVDAC1. B. Single channel recording of a DiphPC/n-decane membrane after the addition of his-tagged purified and refolded hVDAC1. The aqueous phase contained 1 M KCl and 25 ng/ml protein. The applied membrane potential was 10 mV; T = 25 °C. C. Histogram of the conductance steps measured after reconstitution of hVDAC1 into black lipid bilayer membranes; conditions as in B. The most frequent single channel conductance was 4 nS for 123 channels. D. 12% SDS-PAGE of his-tagged hVDAC1Δβ9 expressed in *E. coli* and refolded by a Talon column. M: Mr Markers; 1–6: fractions collected from the Talon column showing the purity of hVDAC1Δβ9. E. Single channel recording of a DiphPC/n-decane membrane after the addition of his-tagged purified and refolded hVDAC1Δβ9. The aqueous phase contained 1 M KCl and 25 ng/ml protein. The applied membrane potential was 10 mV; T = 25 °C. F. Histogram of the conductance steps measured after reconstitution of hVDAC1Δβ9 into black lipid bilayer membranes; conditions as in B. The most frequent single channel conductance was 2 nS for 134 channels. G. 12% SDS-PAGE of his-tagged hVDAC1Δβ9–β10 expressed in *E. coli* and refolded by a Talon column. M: Mr Markers; 1–6: fractions collected from the Talon column showing the purity of hVDAC1Δβ9–β10. H. Single channel recording of a DiphPC/n-decane membrane after the addition of his-tagged purified and refolded hVDAC1Δβ9–β10. The aqueous phase contained 1 M KCl and 25 ng/ml protein. The applied membrane potential was 10 mV; T = 25 °C. I. Histogram of the conductance steps measured after reconstitution of hVDAC1Δβ9 into black lipid bilayer membranes; conditions as in B. The most frequent single channel conductance was 1.5 nS for 58 channels.

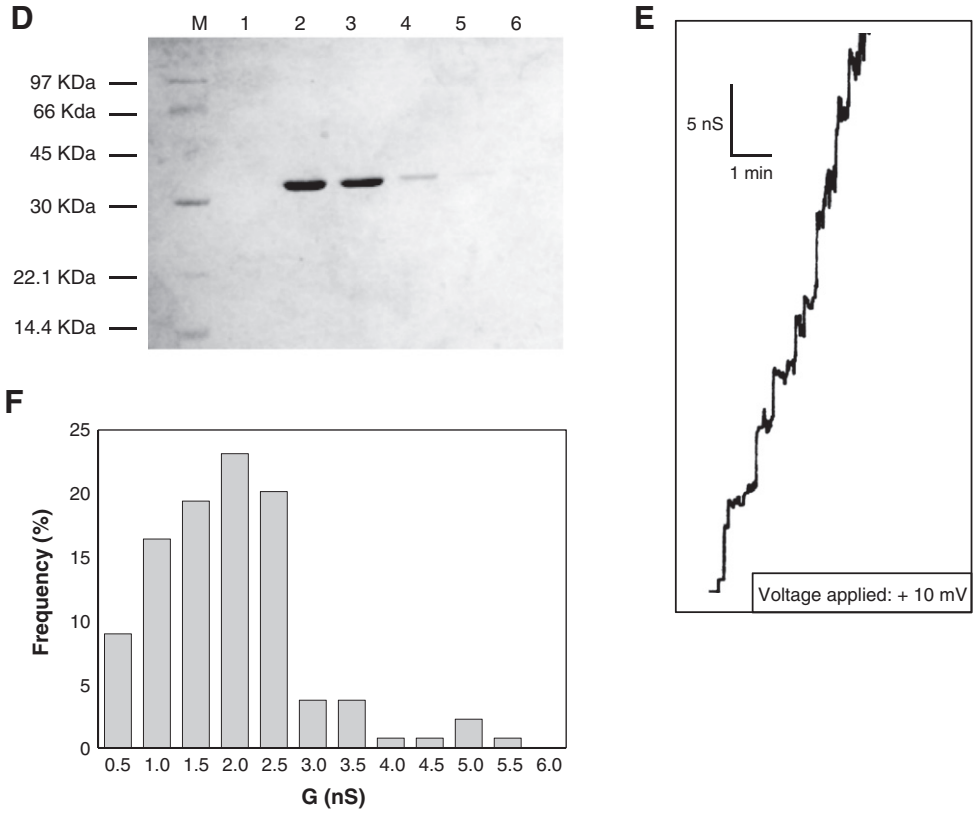

Fig. 7 (*continued*).

The structure of hVDAC1Δβ9–β10 was built based upon changes in the (PDB ID: 3EMN) pdb file [28]. Then, this model was submitted to an MD 200 ns trajectory of the protein embedded in a POPC bilayer and solvated. In Fig. 4 we reported the last snapshot of each system eliminating both the bilayer and the water, for clarity. In Fig. 5 we reported the minimum SASA as a function of time, for the wt hVDAC1 and the mutant, and the respective histograms fitted by Gaussians (see Table 1). As shown, the minimum SASA is constant along the time, suggesting that both structures are stable. The highest probability values point out that the mutant has an area available to ion flows reduced of 1/3 with respect to the VDAC1 (70 (sigma = 16) $Å^2$ vs 192 (sigma = 18) $Å^2$). This indicates that the deletion might reduce the pore diameter (Fig. 4). From the plot of the SASA profile as a function of Z (Fig. 6), it is evident that the deletion decreases the pore uniformly all along the axe Z with the same scale factor. Further, the position of the SASA minimum value is reached for both systems at 7 Å from the center of the pore, corresponding to the region where N-terminal helix folds inside, suggesting a high rigidity of this region that is unperturbed upon mutation.

3.3. The electrophysiological properties of hVDAC1Δβ9 and hVDAC1 Δβ9–β10

3.3.1. Single channel analysis

After dilution in 1% Genapol X-80, the recombinant His-tagged proteins hVDAC1, hVDAC1Δβ9 and hVDAC1Δβ9–β10 were added to the aqueous phase bathing a lipid bilayer membrane. Most of the conductance steps of hVDAC1 had a single channel conductance of 4 nS in 1 M KCl (Fig. 7). Experiments with 0.1 M KCl (not shown) confirmed that single channel conductance was a linear function of the aqueous salt concentration. The single channel properties of hVDAC1 Δβ9 and hVDAC1Δβ9–β10 were different from those of wild type protein (Fig. 7E, H). While the increase in hVDAC1 conductance occurred in distinct steps, the deletion mutants showed "noisy" single channel behavior with fast fluctuations of the channels. The most frequent single channel conductance was 2 nS for hVDAC1Δβ9 and 1.5 nS for hVDAC1 Δβ9–β10 (Fig. 7F, I). These results indicate that the deletion of β-strands leads to proteins forming smaller pores, which are more instable than the wild-type ones. This result was supported by MD simulations.

3.3.2. Voltage-dependence

Fig. 8 shows the analysis of the voltage-dependence of hVDAC1, hVDAC1Δβ9 and hVDAC1Δβ9–β10. The voltage-dependence of recombinant His-tagged hVDAC1 was identical to that measured previously with the protein extracted from yeast mitochondria. Starting with application of about 20–30 mV, the membrane current decreased for both positive and negative potentials, indicating a symmetrical response of the channels to the applied voltage. These results confirm that recombinant hVDAC1 was successfully renatured. hVDAC1Δβ9 showed voltage-dependence similar to that of wild-type protein, although the membrane current decreased more at negative potentials. This asymmetry was even more pronounced in the mutant deleted of both β-strands. Most surprising hVDAC1Δβ9–β10 did not display any voltage-dependence at positive voltages as clearly shown in Fig. 8D. The new functional feature is thus due to the absence of the β-hairpins 9–10.

3.4. Zero-current membrane potential measurements

Zero-current membrane potential experiments with hVDAC1 showed preferential movement of anions through the channel (Table 2), as reported [1–3,53]. In the presence of the chimera N1-VDAC3 the pore became selective for cations over anions. This result cannot be simply explained with change in the protein composition, (ratio positive/negative residues switches from 39 to 35). More

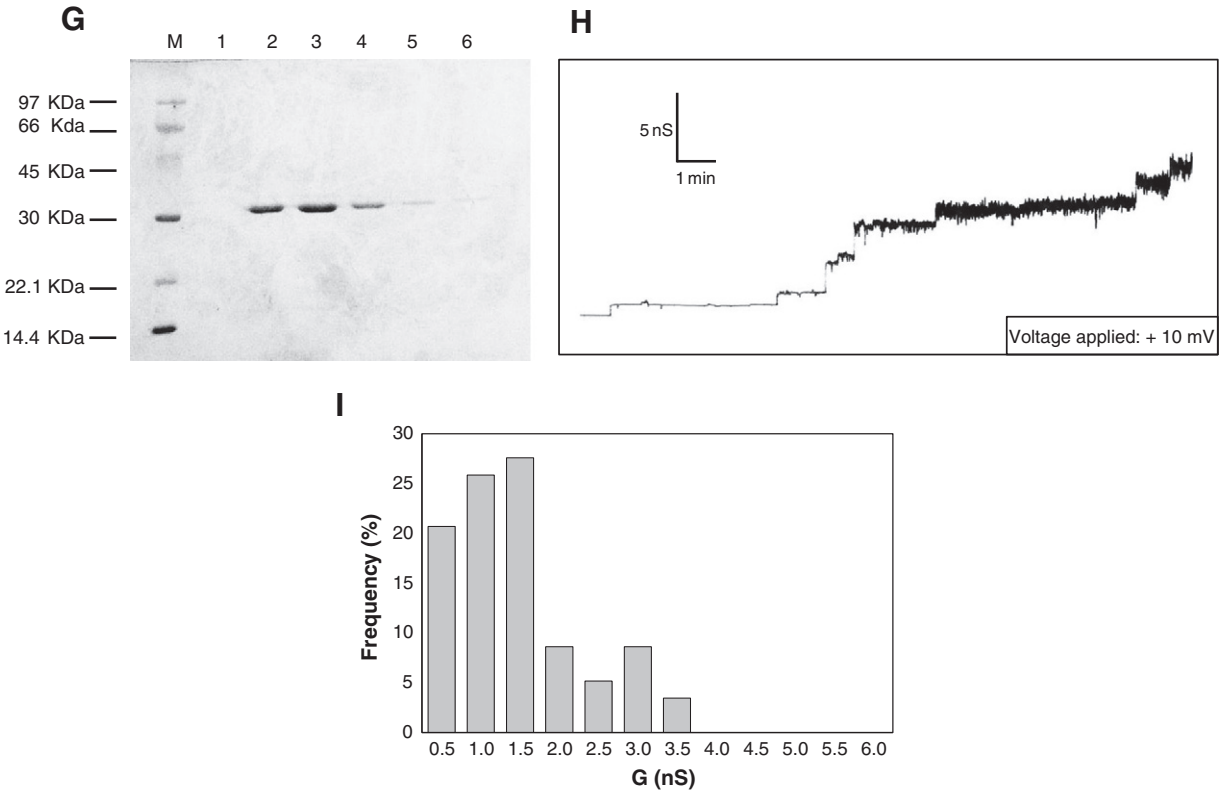

Fig. 7 (*continued*).

interestingly, in the presence of a bulky anion, the cationic selectivity is further enhanced with respect to the controls. This indicated that the screening properties of the pore changed as a consequence of the modifications of the residues exposed to the water-phase. The influence of electrostatic field of the charged residues was shifted by molecular modifications [see 53].

The deletion of one β-strand or one β-hairpin in hVDAC1 produces similar consequences, with a preferential movement of cations in the presence of bulk anions. Also in this mutant the screening features of hVDAC1 have been dramatically altered and the N-terminus defines a narrower section to be flowed by ions. The deletion causes positive residues to approach and this might become a kind of trap for the bulkier anion acetate, thus slowing its movement, as it has been demonstrated by molecular dynamics simulation of the ion flow inside the pore [53].

4. Discussion

The importance of the N-terminal sequence of VDAC1 is witnessed by many reports in the literature devoted to unravel its structure and function (for a detailed list see [54]). The reason for this interest is due to its strategic location and its possible flexibility.

Stemming from the model proposing that hVDAC1 response to voltage is modulated by interaction of the N-terminal region with amino acid residues in the β-strands 9 and 10 [28,32,33], several experiments impacted on the presence and mobility of the N-terminus.

The breakage of the hydrophobic interactions by application of higher voltages has been indicated as responsible for the removal of the N-terminus from inside the pore, causing its lateral "squeezing" and reducing the pore diameter available for ion flux [34]. This model infers that the N-terminal folded inside the pore has a structural function, contributing to the rigidity of the structure (26–28, 32–34). The deletion of the whole N-terminus was reported [8,32,49,54,55]. These mutant pore-protein formed channels, with an evident flickering. Voltage-gating was strongly affected. These data imply that the N-terminal fragment is involved not only in the maintenance of the overall integrity of the incorporated channel, but also in its regulation [55]. It is thus possible to state that also other structural components of the pore, interacting with the N-terminal sequence, might contribute to the regulation of the electrophysiological features of the pore.

In further experimental approaches the immobilization of the N-terminus inside the channel was obtained by introducing mutagenized disulfide bonds [55,56] or by chemical cross-linkers [54].

Following the proposal that Leu10 binds Val143 (β-strand 9, [32]) and Leu150 (β-strand 10, [32]) by hydrophobic interactions, as shown by NMR analyses [32–34], the following couples of disulfide bonds were introduced by mutagenesis of the amino acids: V3-K119 (β-strand 7, [55]), A14-S193 (β-strand 13, [55]), L10-A170 (β-strand 11, [56]); the interactions T6-K197 (β-strand 13, [54]) and T6-K124 were analyzed by cross-linkers (β-strand 8, [54]).

The phenotype of the mutants was different in dependence of the specific change. Cross-linking V3-K119 gave an open channel with similar features than the w.t. but the voltage-dependence had an asymmetric behavior, showing partial closure only when negative voltage was applied to the cis side [55]. In the same work, the disulfide cross-linking between A14 and S193 caused the pore to remain constitutively open [55]. On the opposite, L10-A170 cross-linking mutant displayed native-like channel activity under oxidative conditions: this led the authors to the conclusion that voltage-gating did not involve rearrangements of the N-terminal sequence [56]. The reason for these contradictory data has been discussed in [55]. It is, thus, evident that the interaction between the N-terminus and the pore walls is important in determining the functional phenotype of the pore.

Other examples of site-directed mutagenesis strategy have been used to investigate the influence of specific residues in the electrophysiological features of the pore [57]. In such kind of work not always it is possible to reach definitive conclusions. For example residues K46,

K61, K65 and K84, shown to affect the voltage-sensing mechanism of *S. cerevisiae* VDAC [57], are not conserved in other species. This "graded" mutagenesis is unable to give a clear answer to the basic question of VDAC: what is the mechanism of voltage-gating? We thus imagined introducing more extensive modifications, to profoundly change the interaction pattern of the N-terminus with extensive portions of the pore wall and verify whether these regions are essential for channel formation and voltage-gating.

The first mutant used in this work was a swapping mutant carrying the N-terminus of hVDAC1 inserted on the hVDAC3 barrel [21]. The mutant was purified from yeast mitochondria, after its expression, thus it sustained the maturation process in a eukaryotic contest. It has to be noted that hVDAC3 maintains both V143 and L150 and the N-terminal of hVDAC1 still has in place L10. hVDAC3 also shows conserved Lysines potentially important for the interaction with the N-terminus (K20, K96, K119, K174, K197 or K224) [54]. The swapping mutant has similar pore conductance but lost the voltage-dependence typical of hVDAC1. This can be interpreted as if more residues involved in the interactions between N-terminus and pore walls were changed and this fact de-sensitizes the moiety to move in/out of the pore. The whole electrostatic field due to the network of residues exposed to the hydrophilic inner side of the pore was changed. The voltage sensor has thus been modified so efficiently that it cannot exert its role anymore: this is confirmed by the finding that hVDAC3 appears only poorly or not voltage-dependent [19,20,58].

4.1. Large deletion mutants

Furthermore we designed and generated two hVDAC1 mutants lacking respectively one or two β-strands (Δβ9 and Δβ9–β10). In particular, the deletion of β-strands 9 and 10 can be seen as the deletion of a whole β-hairpin and this does not change the topology of the protein.

It is important to take into account that in hVDAC1Δβ9 the residue V143 has been removed, and in hVDAC1Δβ9–β10 both V143 and L150 were removed: thus their interactions with L10 were made impossible.

To verify that these large deletions were not so harmful to destroy the whole pore structure, we performed a MD simulation of the mutant missing the whole β-hairpin, i.e. hVDAC1Δβ9–β10. The predicted structure was found as stable as the wild type mVDAC1 (PDB ID: 3EMN), but showed a reduced diameter. The deletion of the β-hairpin 9–10 decreased the pore diameter uniformly all along the axe Z with the same scale factor. The region where the N-terminal sequence folds inside is the position where the SASA minimum value was reached for both systems. This indicates a high rigidity of this region that is unperturbed upon mutation and confers to the mutant an elliptical shape.

The electrophysiological data of hVDAC1Δβ9 and hVDAC1 Δβ9–β10 showed that the removal of β9 and β10 in hVDAC1 leads to recombinant proteins forming smaller pores, and MD simulation

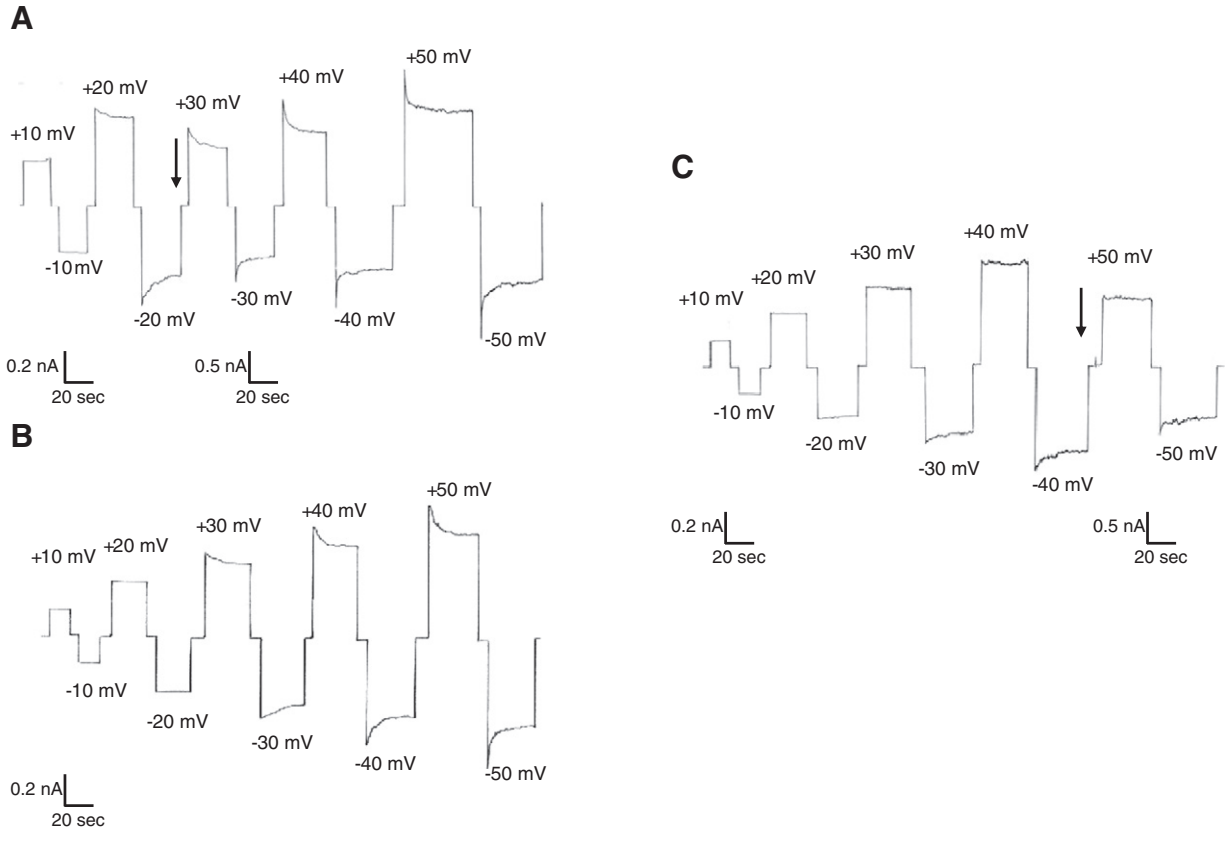

Fig. 8. Voltage-dependence analysis of mutants hVDAC1Δβ9 and hVDAC1Δβ9–β10. Purified proteins were added to the cis side of a DiphPC/n-decane membrane and the incorporation of several channels with a transmembrane potential of 10 mV was followed until the current remained stable. A. Voltage-dependence of purified hVDAC1. Symmetrical voltage steps of linearly increasing amplitude were applied to the membrane, and the membrane current was measured as a function of time. The aqueous phase contained 1 M KCl, T = 25 °C. B. Voltage-dependence of purified hVDAC1Δβ9; conditions as in A. C. Voltage-dependence of purified hVDAC1Δβ9–β10; conditions as in A. D. Analysis of hVDAC1, hVDAC1Δβ9 and hVDAC1Δβ9–β10 voltage-dependence. Ratio of the conductance *G* at a given membrane potential (*V*m) divided by the conductance *G*o at 10 mV as a function of the membrane potential *V*m. The curves show that hVDAC1 is voltage-dependent (full squares). hVDAC1Δβ9–β10 is asymmetrically voltage-dependent, showing to be not sensitive to positive voltages applied to the cis side of the membrane cell. hVDAC1Δβ9 shows an intermediate behavior at positive voltages applied to the cis side. Data are the average of three independent experiments.

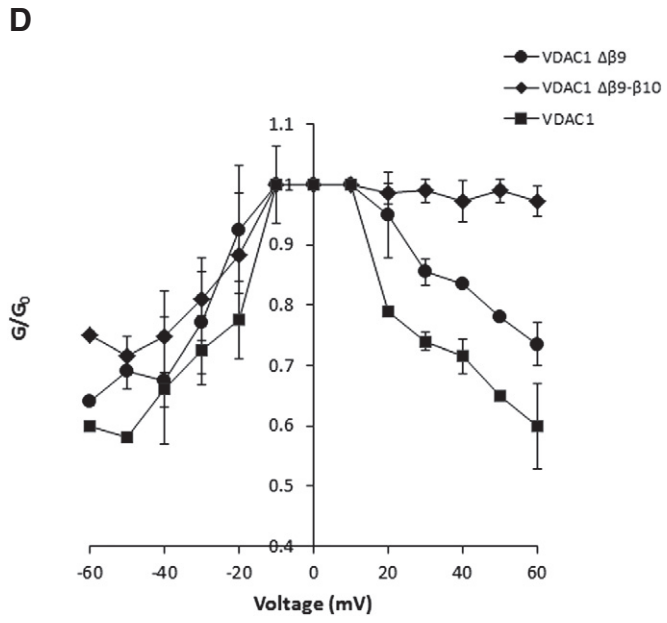

Fig. 8 (*continued*).

supports this conclusion. The most interesting result however is the asymmetric decay of the voltage-dependence of these mutants. In particular, the mutant missing the whole β-hairpin 9–10 has a fully asymmetric behavior, remaining insensitive to positive applied voltages.

4.2. Asymmetric voltage-dependence

In the literature such an asymmetric behavior of voltage-dependence has been rarely observed. One example is upon incubation of hVDAC1 with a synthetic polyanion. The Koenig polyanion (a co-polymer of methacrylate, maleate and styrene) interacts with positive charges on the open mouth of the pore [59,60] and it is able to inhibit the single channel conductance of reconstituted pores [59–61]. Furthermore, the addition of this polyanion on the cis side, upon application of positive, but not negative, potential, resulted in the stabilization of the open state of the pore, i.e. the channel did not close, even when higher voltages were applied to the membrane [59–61]. This result was interpreted as stabilization of the channel in the open state.

The sensitivity to voltage is due to a structure called voltage sensor, containing positive charges or strong dipoles able to move in an electrical field [22–24]. Titration (i.e. by pH changes [62,63]) or lysine residue modification by succinic anhydride [64] can inhibit voltage-gating. The synthetic polyanion has been supposed to produce an asymmetric voltage-dependence because of its interaction with exposed positive residues. This means that Lysines and other basic residues play a decisive role in voltage-dependence.

Mutation of L10 to asparagine slightly affected the voltage-dependence of the pore [34] but in a symmetric fashion. Deletion of the whole N-terminus can fully abolish voltage-dependence, as demonstrated in different reports [49–52,34,65]. The recent finding that cross-linking V3-K119 gives an asymmetrical answer to higher voltage applied [55] agrees with our concept that both N-terminus and sections of the pore walls are essential for the physiological functioning of the pore.

4.3. Voltage-gating: models of mechanism

Presently the two models of the VDAC pore structure are able to justify the physical size and electrophysiological data obtained for the pore in its open conformation [26–29]. VDAC shifts to the so-called closed state (which is indeed not a single state but a series of states all showing a diminished conductance [61,55]), when higher voltages are applied to the membrane. Voltage-gating is nowadays explained with two families of alternative mechanistic hypotheses. In the context of the pore model consisting of 13 β-strands and one transmembrane α-helix [29], the voltage sensor is located at the N-terminal regions 1–80 (one α-helix and 4 β-strands) and it is considered able to move from inside the membrane to out of it, thus reducing the size of the pore diameter [22–24]. If this was true, the asymmetrical voltage-dependence, consequence of the β9–10 hairpin deletion, could be due to hindrance of the re-localization of the voltage sensor outside the pore, but only from one side of it.

More recent evidences, based on the crystal model, have instead mainly focused on the movement of the N-terminal sequence (aa 1–20) [32–34,52,54–56]. In one of these proposals, the N-terminus, folded inside the pore and in contact with the barrel walls, gives structural stability to the open-state, counteracting the lateral pressure exerted on the pore by phospholipids [32–34]. The breakage of hydrophobic interactions by an applied high voltage causes ejection of the N-terminus from within the pore, forcing the channel to partially close because of a lateral membrane stress [34]. Similar conclusions have been drawn by other groups that adopted cross-linking strategies to block the N-terminal mobility (see above).

In our hands, the deletion of the β9–10 hairpin strongly reduces the space available for N-terminus and probably hinders its movement toward outside the pore. This is in agreement with simulations, where the obtained elliptical pore supports a shape controlled by the N-terminal. In addition, the prevalent positive charge of the N-terminus is unfavorable towards movements to one of the two openings of the channel, which shows a prevalence of positive charges delimiting the rim of the pore.

Table 2
Ion selectivity of hVDAC proteins in different salt solutions.

Protein	Pc/Pa		
	KCl	LiCl	CH3COOK pH 7.0
hVDAC1	0.30 ± 0.02	0.35 ± 0.03	0.94 ± 0.016
N1-VDAC3	1.16 ± 0.05	0.57 ± 0.03	1.88 ± 0.17
hVDAC1 Δβ9	0.34 ± 0.04	0.42 ± 0.01	1.58 ± 0.01
hVDAC1 Δβ9–β10	0.51 ± 0.05	0.43 ± 0.02	1.65 ± 0.01

Zero-current membrane potentials, *V*m, of diphytanoyl phosphatidylcholine/n-decane membranes in the presence of hVDAC1, N1-VDAC3, hVDAC1Δβ9 and hVDAC1Δβ9–β10 measured for a 10-fold gradient of different salts. *V*m is defined as the difference between the potential at the dilute side (10 mM) and the potential at the concentrated side (100 mM). The pH of the aqueous salt solutions was 6 unless otherwise indicated; T = 25 °C. The permeability ratio P_{cation}/P_{anion} was calculated with the Goldman–Hodgkin–Katz equation from of at least 3 individual experiments. The application of the GHK equation is an approximation that does not take into account electrostatic effects that might occur in large pores [53]. However the aim of this experiment is to compare this feature under the same conditions and among a limited group of pores.

5. Conclusions

The results obtained from our experiments showed that, according to its crystallographic structure [26–28,32–34] the hVDAC1 pore is stabilized by a network of interactions between the N-terminal and the pore-wall and confirms that interrupting them destroys the voltage-dependence property of this channel. The deletion of β-strand 9 and 10 is consistent with a smaller size of the pore. This was found in our experiments and is supported by structural reconstruction. These two β-strands are candidate to play the most relevant interaction with those regions of the protein involved in the voltage driven re-arrangement and might not move away in the gating of the protein.

Acknowledgements

The financial support of MIUR (PRIN 2010CSJX4F and FIRB-MERIT RBNE08HWLZ) is acknowledged. S.R. was recipient of a FEBS short term fellowship.

References

[1] V. Shoshan-Barmatz, V. De Pinto, M. Zweckstetter, Z. Raviv, N. Keinan, N. Arbel, VDAC, a multi-functional mitochondrial protein regulating cell life and death, Mol. Aspects Med. 31 (2010) 227–285.
[2] R. Benz, Permeation of hydrophilic solutes through mitochondrial outer membranes: review on mitochondrial porins, Biochim. Biophys. Acta 1197 (1994) 167–196.
[3] M. Colombini, VDAC: the channel at the interface between mitochondria and the cytosol, Mol. Cell. Biochem. 256–257 (2004) 107–115.
[4] T. Rostovtseva, M. Colombini, VDAC channels mediate and gate the flow of ATP: implications for the regulation of mitochondrial function, Biophys. J. 72 (1997) 1954–1962.
[5] G. Kroemer, L. Galluzzi, C. Brenner, Mitochondrial membrane permeabilization in cell death, Physiol. Rev. 87 (2007) 99–163.
[6] H. Zaid, S. Abu-Hamad, A. Israelson, I. Nathan, V. Shoshan-Barmatz, The voltage dependent anion channel-1 modulates apoptotic cell death, Cell Death Differ. 12 (2005) 751–760.
[7] T.K. Rostovtseva, B. Antonsson, M. Suzuki, R.J. Youle, M. Colombini, S.M. Bezrukov, Bid, but not Bax, regulates VDAC channels, J. Biol. Chem. 279 (2004) 13575–13583.
[8] F. Tomasello, A. Messina, L. Lartigue, L. Schembri, C. Medina, S. Reina, D. Thoraval, M. Crouzet, F. Ichas, V. De Pinto, F. De Giorgi, Outer membrane VDAC1 controls permeability transition of the inner mitochondrial membrane in cellulo during stress-induced apoptosis, Cell Res. 19 (2009) 1363–1376.
[9] G. Báthori, G. Csordás, C. Garcia-Perez, E. Davies, G. Hajnóczky, Ca^{2+}-dependent control of the permeability properties of the mitochondrial outer membrane and voltage-dependent anion-selective channel (VDAC), J. Biol. Chem. 281 (2006) 17347–17358.
[10] D. De Stefani, A. Bononi, A. Romagnoli, A. Messina, V. De Pinto, P. Pinton, R. Rizzuto, VDAC1 selectively transfers apoptotic Ca(2+) signals to mitochondria, Cell Death Differ. 19 (2012) 267–273.
[11] E.N. Maldonado, J.J. Lemasters, Warburg revisited: regulation of mitochondrial metabolism by voltage-dependent anion channels in cancer cells, J. Pharmacol. Exp. Ther. 342 (2012) 637–641.
[12] N. Arbel, D. Ben-Hail, V. Shoshan-Barmatz, Mediation of the antiapoptotic activity of Bcl-xL protein upon interaction with VDAC1 protein, J. Biol. Chem. 287 (2012) 23152–23161.
[13] V. Shoshan-Barmatz, M. Golan, Mitochondrial VDAC1: function in cell life and death and a target for cancer therapy, Curr. Med. Chem. 19 (2012) 714–735.
[14] P.L. Pedersen, 3-Bromopyruvate (3BP) a fast acting, promising, powerful, specific, and effective "small molecule" anti-cancer agent taken from labside to bedside: introduction to a special issue, J. Bioenerg. Biomembr. 44 (2012) 1–6.
[15] K.S. McCommis, C.P. Baines, The role of VDAC in cell death: friend or foe? Biochim. Biophys. Acta 1818 (2012) 1444–1450.
[16] M. Huizing, W. Ruitenbeek, F. Thinnes, V. De Pinto, Deficiency of the Voltage-Dependent Anion Channel (VDAC): a novel cause of mitochondrial myopathies, Lancet 344 (1994) 762.
[17] M.J. Young, D.C. Bay, G. Hausner, D.A. Court, The evolutionary history of mitochondrial porins, BMC Evol. Biol. 7 (2007) 31.
[18] M. Oliva, A. Messina, G. Ragone, C. Caggese, R. Caizzi, V. De Pinto, Sequence of the *Drosophila melanogaster* mitochondrial porin gene: evidence of a conserved protein domain between fly and mouse, FEBS Lett. 430 (1998) 327–332.
[19] A. Messina, S. Reina, F. Guarino, V. De Pinto, VDAC isoforms in mammals, Biochim. Biophys. Acta 181 (2012) 1466–1476.
[20] V. De Pinto, F. Guarino, A. Guarnera, A. Messina, S. Reina, F.M. Tomasello, V. Palermo, C. Mazzoni, Characterization of human VDAC isoforms: a peculiar function for VDAC3? Biochim. Biophys. Acta 1797 (2010) 1268–1275.
[21] S. Reina, V. Palermo, A. Guarnera, F. Guarino, A. Messina, C. Mazzoni, V. De Pinto, Swapping of the N-terminus of VDAC1 with VDAC3 restores full activity of the channel and confers anti-aging features to the cell, FEBS Lett. 584 (2010) 2837–2844.
[22] M. Colombini, Voltage gating in the mitochondrial channel VDAC, J. Membr. Biol. 111 (1989) 103–111.
[23] J. Song, C. Midson, E. Blachly-Dyson, M. Forte, M. Colombini, The topology of VDAC as probed by biotin modification, J. Biol. Chem. 273 (1998) 24406–24413.
[24] J. Song, C. Midson, E. Blachly-Dyson, M. Forte, M. Colombini, The sensor regions of VDAC are translocated from within the membrane to the surface during the gating processes, Biophys. J. 74 (1998) 2926–2944.
[25] R. Benz, M. Kottke, D. Brdiczka, The cationically selective state of the mitochondrial outer membrane pore: a study with intact mitochondria and reconstituted mitochondrial porin, Biochim. Biophys. Acta 1022 (1990) 311–318.
[26] S. Hiller, R.G. Garces, T.J. Malia, V.Y. Orekhov, M. Colombini, G. Wagner, Solution structure of the integral human membrane protein VDAC-1 in detergent micelles, Science 321 (2008) 1206–1210.
[27] M. Bayrhuber, T. Meins, M. Habeck, S. Becker, K. Giller, S. Villinger, C. Vonrhein, C. Griesinger, M. Zweckstetter, K. Zeth, Structure of the human voltage-dependent anion channel, Proc. Natl. Acad. Sci. U. S. A. 105 (2008) 15370–15375.
[28] R. Ujwal, D. Cascio, J.P. Colletier, S. Faham, J. Zhang, L. Toro, P. Ping, J. Abramson, The crystal structure of mouse VDAC1 at 2.3 angstrom resolution reveals mechanistic insights into metabolite gating, Proc. Natl. Acad. Sci. U. S. A. 105 (2008) 17742–17747.
[29] M. Colombini, The published 3D structure of the VDAC channel: native or not? Trends Biochem. Sci. 34 (2009) 382–389.
[30] S. Hiller, J. Abramson, C. Mannella, G. Wagner, K. Zeth, The 3D structures of VDAC represent a native conformation, Trends Biochem. Sci. 35 (2010) 514–521.
[31] V. De Pinto, F. Tomasello, A. Messina, F. Guarino, R. Benz, D. La Mendola, A. Magrì, D. Milardi, G. Pappalardo, Determination of the conformation of the human VDAC1 N-terminal peptide, a protein moiety essential for the functional properties of the pore, Chembiochem 8 (2007) 744–756.
[32] R. Schneider, M. Etzkorn, K. Giller, V. Daebel, J. Eisfeld, M. Zweckstetter, C. Griesinger, S. Becker, A. Lange, The native conformation of the human VDAC1 N terminus, Angew. Chem. Int. Ed Engl. 49 (2010) 1882–1885.
[33] S. Villinger, R. Briones, K. Giller, U. Zachariae, A. Lange, B.L. de Groot, C. Griesinger, S. Becker, M. Zweckstetter, Functional dynamics in the voltage-dependent anion channel, Proc. Natl. Acad. Sci. U. S. A. 107 (2010) 22546–22551.
[34] U. Zachariae, R. Schneider, R. Briones, Z. Gattin, J.P. Demers, K. Giller, E. Maier, M. Zweckstetter, C. Griesinger, S. Becker, R. Benz, B.L. de Groot, A. Lange, β-Barrel mobility underlies closure of the voltage-dependent anion channel, Structure 20 (2012) 1540–1549.
[35] G.A. Reid, Effects of nitrogen supplements on degradation of aspen wood lignin and carbohydrate components by *Phanerochaete chrysosporium*, Methods Enzymol. 97 (1983) 324–329.
[36] M. Suissa, K. Suda, G. Schatz, Isolation of the nuclear yeast genes for citrate synthase and fifteen other mitochondrial proteins by a new screening method, EMBO J. 3 (1984) 1773–1781.
[37] C. Gregg, P. Kyryakov, V.I. Titorenko, Purification of mitochondria from yeast cells, J. Vis. Exp. 30 (2009) e1417.
[38] V. De Pinto, R. Benz, F. Palmieri, Interaction of non-classical detergents with the mitochondrial porin: a new purification procedure and characterization of the pore-forming unit, Eur. J. Biochem. 183 (1989) 179–187.
[39] S.N. Ho, H.D. Hunt, R.M. Horton, J.K. Pullen, L.R. Pease, Site-directed mutagenesis by overlap extension using the polymerase chain reaction, Gene 77 (1989) 51–59.
[40] R.M. Horton, H.D. Hunt, S.N. Ho, J.K. Pullen, L.R. Pease, Engineering hybrid genes without the use of restriction enzymes: gene splicing by overlap extension, Gene 77 (1989) 61–68.
[41] Y. Shi, C. Jiang, Q. Chen, H. Tang, One-step on-column affinity refolding purification and functional analysis of recombinant human VDAC1, Biochem. Biophys. Res. Commun. 303 (2003) 475–482.
[42] R. Benz, K. Janko, W. Boos, P. Läuger, Formation of large, ion-permeable membrane channels by the matrix protein (porin) of *Escherichia coli*, Biochim. Biophys. Acta 511 (1978) 305–319.
[43] R. Benz, A. Schmid, R.E. Hancock, Ion selectivity of gram-negative bacterial porins, J. Bacteriol. 162 (1985) 722–727.
[44] K. Lindorff-Larsen, S. Piana, K. Palmo, P. Maragakis, J.L. Klepeis, Improved side-chain torsion potentials for the Amber ff99SB protein force field, Proteins 78 (2010) 1950–1958.
[45] B. Jojart, T.A. Martinek, Performance of the general amber force field in modeling aqueous POPC membrane bilayers, J. Comput. Chem. 28 (2007) 2051–2058.
[46] A. Fiser, A. Sali, Modeller: generation and refinement of homology-based protein structure models, Methods Enzymol. 374 (2003) 461–491.
[47] M.J. Harvey, G. Giupponi, G. De Fabritiis, ACEMD: accelerating biomolecular dynamics in the microsecond time scale, J. Chem. Theory Comput. 5 (2009) 1632–1639.
[48] A. Kumar, E. Hajjar, P. Ruggerone, M. Ceccarelli, Molecular simulations reveal the mechanism and the determinants for ampicillin translocation through OmpF, J. Phys. Chem. 114 (2010) 9608–9616.
[49] B. Popp, D.A. Court, R. Benz, W. Neupert, R. Lill, The role of the N and C termini of recombinant *Neurospora* mitochondrial porin in channel formation and voltage-dependent gating, J. Biol. Chem. 271 (1996) 13593–13599.
[50] D.A. Koppel, K.W. Kinnally, P. Masters, M. Forte, E. Blachly-Dyson, C.A. Mannella, Bacterial expression and characterization of the mitochondrial outer membrane channel. Effects of N-terminal modifications, J. Biol. Chem. 273 (1998) 13794–13800.
[51] G. Runke, E. Maier, W.A. Summers, D.C. Bay, R. Benz, D.A. Court, Deletion variants of *Neurospora* mitochondrial porin: electrophysiological and spectroscopic analysis, Biophys. J. 90 (2006) 3155–3164.
[52] S. Abu-Hamad, N. Arbel, D. Calo, L. Arzoine, A. Israelson, N. Keinan, R. Ben-Romano, O. Friedman, V. Shoshan-Barmatz, The VDAC1 N-terminus is essential both for apoptosis and the protective effect of anti-apoptotic proteins, J. Cell Sci. 122 (2009) 1906–1916.
[53] E.M. Krammer, F. Homblé, M. Prévost, Concentration dependent ion selectivity in VDAC: a molecular dynamics simulation study, PLoS One 6 (2011) e27994.
[54] S. Geula, D. Ben-Hail, V. Shoshan-Barmatz, Structure-based analysis of VDAC1: N-terminus location, translocation, channel gating and association with anti-apoptotic proteins, Biochem. J. 444 (2012) 475–485.
[55] B. Mertins, G. Psakis, W. Grosse, K.C. Back, A. Salisowski, et al., Flexibility of the N-terminal mVDAC1 segment controls the channel's gating behavior, PLoS One 7 (2012) e47938.
[56] O. Teijido, R. Ujwal, C.O. Hillerdal, L. Kullman, T.K. Rostovtseva, J. Abramson, Affixing the N-terminal alpha helix of the voltage dependent anion channel to the channel's wall does not prevent its voltage gating, J. Biol. Chem. 287 (2012) 11437–11445.
[57] L. Thomas, E. Blachly-Dyson, M. Colombini, M. Forte, Mapping of residues forming the voltage sensor of the voltage-dependent anion-selective channel, Proc. Natl. Acad. Sci. U. S. A. 90 (1993) 5446–5449.

[58] X. Xu, W. Decker, M.J. Sampson, W.J. Craigen, M. Colombini, Mouse VDAC isoforms expressed in yeast: channel properties and their roles in mitochondrial outer membrane permeability, J. Membr. Biol. 170 (1999) 89–102.
[59] R. Benz, L. Wojtczak, W. Bosch, D. Brdiczka, Inhibition of adenine nucleotide transport through the mitochondrial porin by a synthetic polyanion, FEBS Lett. 231 (1988) 75–80.
[60] M. Colombini, C.L. Yeung, J. Tung, T. König, The mitochondrial outer membrane channel, VDAC, is regulated by a synthetic polyanion, Biochim. Biophys. Acta 905 (1987) 279–286.
[61] G. Bàthori, I. Szabo, I. Schmehl, F. Tombola, A. Messina, V. De Pinto, M. Zoratti, Novel aspects of the electrophysiology of mitochondrial porin, Biochem. Biophys. Res. Commun. 243 (1998) 258–263.
[62] K.A. Bowen, K. Tam, M. Colombini, Evidence for titratable gating charges controlling the voltage dependence of the outer mitochondrial membrane channel, VDAC, J. Membr. Biol. 86 (1985) 51–59.
[63] V. De Pinto, J.A. Al Jamal, R. Benz, F. Palmieri, Positive residues involved in the voltage-gating of the mitochondrial porin-channel are localized in the external moiety of the pore, FEBS Lett. 274 (1990) 122–126.
[64] C. Doring, M. Colombini, The mitochondrial voltage-dependent channel, VDAC, is modified asymmetrically by succinic anhydride, J. Membr. Biol. 83 (1985) 87–94.
[65] V. De Pinto, S. Reina, F. Guarino, A. Messina, The structure of voltage-dependent anion selective channel: state of the art, J. Bioenerg. Biomembr. 40 (2008) 139–147.